
Foundation Model for Chemical Process Modeling: Meta-Learning with Physics-Informed Adaptation

Zihao Wang

National University of Singapore
e0424629@u.nus.edu

Zhe Wu

National University of Singapore
wuzhe@nus.edu.sg

Abstract

In this work, we introduce a novel application of foundation models in the domain of nonlinear chemical process modeling. Given the challenges of obtaining accurate first-principles models for real-world chemical processes and the inefficiency of rebuilding and retraining models for new chemical processes, we pose a pivotal question: What if we could develop a single, universal neural network (i.e., foundation model) capable of rapidly adapting to modeling any new chemical process? To address this question, we propose a meta-learning-based approach using Reptile to construct the foundation model, followed by physics-informed adaptation to fine-tune it to new modeling tasks using only a few data samples. To assess the effectiveness of our methodology, we construct a foundation model for various chemical reactions in three classical generic reactors, including continuous stirred tank reactors (CSTRs), batch reactors (BRs), and plug flow reactors (PFRs). Our approach outperforms conventional methods such as data-driven learning, physics-informed learning, transfer learning, and pure meta-learning in a few-shot setting. Furthermore, our method achieves rapid adaptation to new CSTRs, BRs, and PFRs using only a few data samples from the designated tasks. Source code is available at <https://github.com/killingbear999/chemical-process-foundation-model>.

1 Introduction

Research on foundation models has made significant progress in recent years. The term “foundation model” refers to any model trained on broad data, capable of adaptation (e.g., fine-tuning) to a broad spectrum of downstream tasks [1]. The success of foundation models in computer science, such as ChatGPT in natural language processing [2] and Sora in computer vision [3], has spurred their applications in traditional engineering disciplines such as material science [4] and biomolecular engineering [5, 6], and natural sciences such as astronomy [7] and physics [8].

However, research on foundation models in chemical engineering is currently sparse, but is essential [9]. Some works have been done to build foundation models for answering chemistry-related scientific questions [10] and solving various chemical and biological tasks such as answering biomedical questions and molecular synthesis [11]. It should be noted that much of the existing research frames the problem as a linguistic one, constructing foundation models primarily as Large Language Models (LLMs), which offers limited support for advancing chemical-related research. Therefore, we are motivated to bridge this gap by developing a chemical-related foundation model capable of modeling a wide range of chemical processes in classical reactors. Our aim is to address the challenges associated with modeling of nonlinear chemical processes in an effective and efficient manner.

Modeling of chemical reactions in real-world scenarios is pivotal for various applications, such as process monitoring, optimization, and advanced process control. Given the challenges associated with obtaining first-principles models for complex chemical reactions, there has been a transition to utilize data-driven methods such as machine learning-based models to capture the system dynamics

of chemical reactions [12, 13, 14]. However, a significant hurdle in employing deep learning within scientific domains is the scarcity of experimental data, which is normally costly and time-consuming to acquire via physical experimentation (e.g., it is resource-intensive to collect data and build neural network models for every new chemical reaction). To mitigate this challenge, transfer learning-based approaches have been suggested [15, 16]. Nonetheless, for transfer learning-based methods, the process of identifying analogous reactions with adequate data, pre-training, and then transferring to the designated reaction must be repeated for each new reaction with a considerable number of samples, typically hundreds or thousands [17].

This prompts the question: what if we develop **ONE** universal neural network capable of swiftly adapting to any new reaction? For instance, we can train such a universal neural network to encompass various chemical reactions in traditional types of reactors such as continuous stirred tank reactors (CSTRs), batch reactors (BRs), and plug flow reactors (PFRs) that are commonly used in chemical engineering. When confronted with a new reaction in a specific type of reactor, a mere handful of samples would suffice to fine-tune the pre-trained model, thereby enabling it to adapt to the specific reaction. Since this methodology aligns with the concept of few-shot learning in image classification, we will use the term "few-shot adaptation" to define our goal here. In this work, the term "shot" is used interchangeably with "sample". Specifically, our goal is to train a foundation model on diverse datasets comprising various chemical reactions in CSTRs, BRs, and PFRs. The model will then be fine-tuned with a minimal number of samples from new tasks, enabling rapid adaptation to specific chemical reactions. The high-level system architecture is shown in Fig. 1.

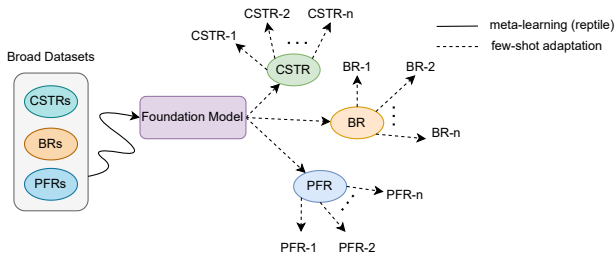


Figure 1: High-level system architecture of foundation model for various chemical reactors.

To address the aforementioned question, we employ a meta-learning technique to build the foundation model, specifically Reptile [18]. After acquiring the foundation model through Reptile, a conventional method to adapt the model to any new processes is via few-shot adaptation. However, purely data-driven adaptation may lead to poor generalization performance for nonlinear systems due to its complex dynamics in state-space. Therefore, to improve the generalizability of the foundation model and reduce the amount of data for adaptation, we propose a physics-informed few-shot adaptation approach by incorporating physics knowledge such as governing equations (e.g., mass and energy balance equations) into the adaptation process. To demonstrate the effectiveness of the proposed method, simulation data of hundreds of different reactions in three classical reactors is used to develop the foundation model that will be further adapted to new reaction processes with limited data available. It is demonstrated that the adaptation process from the foundation model to a specific reaction becomes more efficient, requiring fewer shots for successful adaptation under the proposed physics-informed framework.

The rest of this article is organized as follows: Section 2 develops the Reptile-based foundation model with physics-informed adaptation. Section 3 introduces the formulation of CSTRs, BRs, and PFRs, including reactor modeling and design of physics-informed loss functions. Section 4 evaluates the few-shot performance of our proposed method to new CSTRs, BRs, and PFRs. Section 5 discusses the limitations of the current design and suggests potential directions for future research.

2 Reptile with physics-informed few-shot adaptation

2.1 Class of systems

In this work, we consider chemical processes that can be described by the following class of nonlinear ordinary differential equations (ODEs):

$$\dot{x} = F(x, u) \quad (1)$$

where $x \in \mathbb{R}^n$ denotes the state vector (e.g., temperature, concentration, etc.), $u \in \mathbb{R}^m$ is the control input vector (e.g., adjusting feed rate and composition, etc.). $F : D \times U \rightarrow \mathbb{R}^n$ is \mathcal{C}^1 , where $D \subset \mathbb{R}^n$ and $U \subset \mathbb{R}^m$ are compact and connected subsets that contain an open neighborhood of the origin, respectively. Since first-principles models may not be available for complex real-world systems, our goal is to develop a neural network for the nonlinear system of Eq. 1.

2.2 Methodology

In this section, we present an outline of our methodology aimed at achieving the objective highlighted in the Introduction. Unlike LLMs such as ChatGPT, our approach tackles the problem through meta-learning rather than reinforcement learning. Specifically, we employ an algorithm called Reptile [18]. Reptile serves as a simplified version of Model-Agnostic Meta-Learning (MAML) [19] and its variants [20, 21, 22, 23]. Both MAMLs and Reptile are training algorithms designed to optimize neural network weights, facilitating easy adaptation to new tasks with just a few shots from those tasks. Additionally, Reptile stands out for its computational efficiency, which is a crucial evaluation criteria for real-world applications, utilizing only first-order derivatives for meta-learning updates, whereas MAML employs second-order derivatives [24]. In short, Reptile finds network parameters θ such that the Euclidean distance $\mathcal{D}(\theta, \mathcal{W}_\tau)$ is minimized for all tasks (i.e., finding a point near all solution manifolds), where \mathcal{W}_τ is the set of optimal parameters for task τ (i.e., the detailed mathematical reasoning on why Reptile works can be found in [24]):

$$\min_{\theta} \mathbb{E}_{\tau} [\frac{1}{2} \mathcal{D}(\theta, \mathcal{W}_{\tau})^2]$$

In our case, the task τ represents specific chemical processes represented by the ODEs of Eq. (1). Analogously, Reptile operates akin to a **tug-of-war** scenario, where task groups exert force in different directions, striving to establish equilibrium, ultimately achieving a balanced state in the system (i.e., a concept reminiscent of static equilibrium in Physics).

Our methodology comprises two distinct phases: meta-training and meta-testing. During meta-training, we immerse the model (i.e., specifically, a recurrent neural network (RNN)) in a diverse array of chemical reactions across various reactor types. In short, the meta-training process involves two steps. First, we obtain the optimal parameters \mathcal{W}_τ for a specific task τ using mean-squared error (MSE) and the Adam optimizer (i.e., since we are performing regression). Once \mathcal{W}_τ is determined, we update the network parameters θ using the Reptile update rule:

$$\theta \leftarrow \theta + \epsilon(\mathcal{W}_{\tau} - \theta)$$

where ϵ is the meta-optimization step size hyperparameter. This process is then repeated recursively for all tasks. Since Reptile has been well-studied, further discussion on Reptile and the detailed meta-training Algorithm 2 are provided in Appendix A.

In the subsequent meta-testing phase, we select previously unseen chemical reactions and undertake physics-informed few-shot adaptations to them, respectively, leveraging the Reptile-based foundation model obtained during meta-training, as outlined in Algorithm 1. It should be pointed out that we use few-shot data x (i.e., $x \in \mathcal{X} \subset D$, where \mathcal{X} denotes the set of few-shot training data) to compute the data-driven loss term \mathcal{L}_d and use collocation points x_c (i.e., $x_c \in \mathcal{X}_c \subset D$, where \mathcal{X}_c denotes the set of collocation data points, and $\mathcal{X} \cap \mathcal{X}_c = \emptyset$) to compute the physics-informed loss term \mathcal{L}_p in Algorithm 1 (i.e., a collocation point refers to a specific location within the domain of interest where the governing physics equations are enforced as part of the training process). As we do not utilize any labeled output data for \mathcal{L}_p , there is no need to perform physical experiments to gather additional data, which remains consistent with our few-shot setting. The detailed formulation of physics-informed loss functions with respect to CSTRs, BRs, and PFRs will be presented in Section 3, along with the first-principles models of CSTRs, BRs, and PFRs for better understanding. Moreover, a detailed discussion on physics-informed neural networks (PINNs) is provided in Appendix C.1.

3 Foundation model for chemical processes

In this section, we develop a foundation model following Algorithm 1 and Algorithm 2 to learn the dynamics of various chemical reactions in three types of reactors. We first present the formulation of CSTRs, BRs, and PFRs, alongside their corresponding physics-informed loss functions. In this

Algorithm 1 Physics-Informed Few-Shot Adaptation

Require: $p(\mathcal{T})$: distribution over tasks;
Require: γ_1, γ_2 : loss function weighting hyperparameters;
Require: x, y : few-shot inputs and outputs respectively;
Require: x_c : collocation points
Require: $Model$: pre-trained foundation model;
 1: Sample an unseen task $\tau \sim p(\mathcal{T})$;
 2: Load the parameters θ from $Model$;
 3: **for** $epoch \leftarrow 1, 2, \dots, n_{epochs}$ **do**
 4: **for** $i \leftarrow 1, 2, \dots, n_{batches}$ **do** $\triangleright n_{batches} = 1$ normally due to few-shot inputs
 5: $\tilde{y}_i \leftarrow Model(x_i)$; $\triangleright \tilde{y}_i$ is the predicted output w.r.t current batch of few-shot input x_i
 6: $\tilde{y}_p \leftarrow Model(x_c)$; $\triangleright \tilde{y}_p$ is the predicted output w.r.t x_c
 7: Compute loss $\mathcal{L}_{\tau_i} \leftarrow \gamma_1 \mathcal{L}_{\tau_d}(\tilde{y}_i, y_i) + \gamma_2 \mathcal{L}_{\tau_p}(\tilde{y}_p, x_c)$ w.r.t. current batch;
 8: Update $\theta \leftarrow Adam(\mathcal{L}_{\tau_i}, \theta)$;
 9: **end for**
 10: **end for**

work, we utilize the notations CSTRs, BRs, and PFRs to distinguish between different chemical reactions for easy reference (e.g., CSTRs denote multiple different CSTR-based chemical reactions). Furthermore, within the scope of this paper, we only considered elementary chemical reactions that transform reactant A to product B (irreversible reaction) for all three types of reactors. Specifically, we consider CSTRs and BRs with a second-order reaction from A to B, and PFR with a first-order reaction from A to B to demonstrate the capability of the proposed modeling method for handling various elementary reactions with different orders and in different reactors. The schematic of the three reactors is shown in Fig. 2. However, it should be mentioned that the proposed method can be generalized to more diverse reactions, provided that the dataset is available. A further discussion on reactor modeling is included in Appendix C.2 and physics-informed loss function is included in Appendix C.3. Moreover, the specific parameter value ranges for CSTRs, BRs, and PFRs are described in Appendix B.

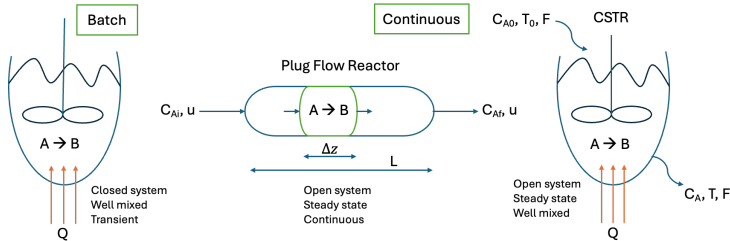


Figure 2: Schematic of reactors.

3.1 CSTR modeling and physics-informed loss function

The CSTR is equipped with a heating jacket that supplies/removes heat at a rate Q . The CSTR dynamic model is described by the following material and energy balance equations:

$$\frac{dC_A}{dt} = \frac{F}{V}(C_{A0} - C_A) - k_0 e^{-\frac{E}{RT}} C_A^2, \quad \frac{dT}{dt} = \frac{F}{V}(T_0 - T) + \frac{-\Delta H}{\rho_L C_p} k_0 e^{-\frac{E}{RT}} C_A^2 + \frac{Q}{\rho_L C_p V} \quad (2)$$

where C_A is the concentration of reactant A, V is the volume of the reacting liquid, T is the temperature, Q is the heat input rate, C_{A0} is the inlet concentration of reactant A, T_0 is the inlet temperature, F is the volumetric flow rate, ρ_L is the constant density of the reacting liquid, C_p is the heat capacity, ΔH is the enthalpy of reaction, k_0 is the pre-exponential constant, E is the activation energy, and R is the ideal gas constant. The manipulated inputs (i.e., control) in this system are represented by $\Delta C_{A0} = C_{A0} - C_{A0_s}$ and $\Delta Q = Q - Q_s$, such that the equilibrium point of the system is located at the origin of the state-space. Also, in this case study, T , C_A , ΔQ , ΔC_{A0} are evenly sampled from $[300, 600] K$, $[0, 6] kmol/m^3$, $[-5, 5] \times 10^5 kJ/hr$, and $[-3.5, 3.5] kmol/m^3$ respectively. However, it is noted that the ranges of variables can be chosen appropriately for the foundation model depending on the operating conditions of interest.

In the context of CSTR modeling, the inputs consist of $[T_t, C_{A_t}, Q_t, C_{A0_t}]$ at the current time step t . The outputs entail the state trajectory $[T_{t+1, \dots, n}, C_{A_{t+1, \dots, n}}]$ over the subsequent n time steps (i.e., representing a one-to-many sequence problem). Leveraging parameter values randomly drawn from the range delineated in Table 1 in Appendix B, and employing the material and energy balance equations depicted in Eq. (2), we conduct numerical simulations of diverse CSTRs to collect their respective output sequences, which involve employing the explicit Euler method with an integration time step of $h_c = 1 \times 10^{-4} \text{ hr}$, relative to a sampling period of $\Delta = 5 \times 10^{-3} \text{ hr}$.

Subsequently, when implementing the foundation model to a new process (e.g., a new reaction in a CSTR), we will apply physics-informed adaptation method. Specifically, the physics-informed loss function for learning a new CSTR is the weighted sum of data-driven loss term \mathcal{L}_d and physics-informed loss term \mathcal{L}_p . \mathcal{L}_d takes the form of MSE of the actual output y and the predicted output \tilde{y} using the actual few-shot data. \mathcal{L}_p is defined as the weighted sum of two terms, namely loss term with respect to predicted concentration \mathcal{L}_{C_A} and loss term with respect to predicted temperature \mathcal{L}_T , and it is expressed as follows:

$$\mathcal{L}_p = \gamma_1 \mathcal{L}_{C_A} + \gamma_2 \mathcal{L}_T = \gamma_1 \frac{1}{n} \sum_{i=1}^n \mathcal{L}_{C_{A_{t+i}}}^2 + \gamma_2 \frac{1}{n} \sum_{i=1}^n \mathcal{L}_{T_{t+i}}^2 \quad (3)$$

where

$$\mathcal{L}_{C_{A_{t+i}}} = \frac{d\tilde{C}_{A_{t+i}}}{dt} - \frac{F}{V}(C_{A0_t} - \tilde{C}_{A_{t+i}}) + k_0 e^{\frac{-E}{RT_{t+i}}} \tilde{C}_{A_{t+i}}^2 \quad (4a)$$

$$\mathcal{L}_{T_{t+i}} = \frac{d\tilde{T}_{t+i}}{dt} - \frac{F}{V}(T_0 - \tilde{T}_{t+i}) + \frac{\Delta H}{\rho_L C_p} k_0 e^{\frac{-E}{RT_{t+i}}} \tilde{C}_{A_{t+i}}^2 - \frac{Q_t}{\rho_L C_p V} \quad (4b)$$

We compute the physics-informed loss term utilizing collocation points only rather than relying on few-shot data. Here, \tilde{C}_A and \tilde{T} represent the predicted outputs corresponding to the collocation points as inputs and we use explicit Euler method for solving the ODEs. When operating a real-world CSTR, certain parameters such as F, V, T_0, C_{A0_s} , and Q_s are typically known through expert knowledge and direct physical measurements. However, other critical parameters, such as $k_0, E, \Delta H, C_p$, and ρ_L , may not be directly measurable and thus remain unknown. To compute \mathcal{L}_p , we utilize the actual values of F, V, T_0, C_{A0_s} , and Q_s , while estimating the values of $k_0, E, \Delta H, C_p$, and ρ_L in Eq. (4). Specifically, we used the median values of $k_0, E, \Delta H, C_p$, and ρ_L from their respective sampling ranges shown in Table 1 in Appendix B.

3.2 BR modeling and physics-informed loss function

The BR is equipped with a heating jacket that supplies/removes heat at a rate Q . The BR dynamic model is described by the following material and energy balance equations:

$$\frac{dC_A}{dt} = -k_0 e^{\frac{-E}{RT}} C_A, \quad \frac{dT}{dt} = \frac{-\Delta H}{\rho_L C_p} k_0 e^{\frac{-E}{RT}} C_A + \frac{Q}{\rho_L C_p V} \quad (5)$$

where the notations follow those for CSTRs, and are omitted here. T, C_A, Q are evenly sampled from $[300, 600] \text{ K}$, $[0, 6] \text{ kmol/m}^3$, and $[-5, 5] \times 10^5 \text{ kJ/hr}$ respectively. In the context of BR modeling, to maintain uniform input dimensions akin to CSTRs, we implement padding on the inputs for BRs. Consequently, the final inputs comprise $[T_t, C_{A_t}, Q_t, Q_t]$ at the current time step t , while the outputs encapsulate the state trajectory $[T_{t+1, \dots, n}, C_{A_{t+1, \dots, n}}]$ over the subsequent n time steps (i.e., representing a one-to-many sequence problem). Leveraging parameter values randomly drawn from the range delineated in Table 2 in Appendix B, and employing the material and energy balance equations depicted in Eq. (5), we conduct numerical simulations of diverse BRs to collect their respective output sequences, which involve employing the explicit Euler method with an integration time step of $h_c = 1 \times 10^{-4} \text{ hr}$, relative to a sampling period of $\Delta = 5 \times 10^{-2} \text{ hr}$.

The BR physics-informed loss function is the weighted sum of data-driven loss term \mathcal{L}_d and physics-informed loss term \mathcal{L}_p . \mathcal{L}_d and \mathcal{L}_p take similar forms as those for CSTRs (i.e., Eq. (3)) but with different $\mathcal{L}_{C_{A_{t+i}}}$ and $\mathcal{L}_{T_{t+i}}$, where

$$\mathcal{L}_{C_{A_{t+i}}} = \frac{d\tilde{C}_{A_{t+i}}}{dt} + k_0 e^{\frac{-E}{RT_{t+i}}} \tilde{C}_{A_{t+i}}, \quad \mathcal{L}_{T_{t+i}} = \frac{d\tilde{T}_{t+i}}{dt} + \frac{\Delta H}{\rho_L C_p} k_0 e^{\frac{-E}{RT_{t+i}}} \tilde{C}_{A_{t+i}} - \frac{Q_t}{\rho_L C_p V} \quad (6)$$

Similar to CSTRs, we compute the physics-informed loss term utilizing collocation points only rather than relying on few-shot data. Additionally, given a new BR, we also assume that the actual values of V and Q are known, while the values of k_0 , E , ΔH , C_p , and ρ_L remain unknown and will be estimated (i.e., using the median values from their respective sampling ranges shown in Table 2) in Appendix B in Eq. (6) for model adaptation.

3.3 PFR modeling and physics-informed loss function

The PFR dynamic model is described by a set of partial differential equations (PDEs) (i.e., detailed in Appendix B). To solve PDEs for the PFR model, we employ the method of lines. Specifically, we discretize the reactor in length to approximate the spatial derivatives through finite differences which results in a set of coupled ODEs (i.e., discretizing reactor length L into N sub-parts). These ODEs are subsequently solved using Euler method to obtain future states for one sampling period along the reactor length, as depicted in Eq.(7):

$$\frac{dC_{A_N}}{dt} = -u \frac{C_{A_N} - C_{A_{N-1}}}{Z_{N-1} - Z_N} - k_0 e^{\frac{-E}{RT}} C_A \quad (7a)$$

$$\frac{dT_N}{dt} = -u \frac{T_N - T_{N-1}}{Z_{N-1} - Z_N} + \frac{-\Delta H}{\rho_L C_p} k_0 e^{\frac{-E}{RT}} C_A + \frac{U}{\rho_L C_p A} A_c (T_c - T) \quad (7b)$$

where Z is the discretized elements (i.e., $N - 1$ evenly spaced numbers over a specified reactor length L), U is the overall heat transfer coefficient, u is the superficial velocity, T_c is the cooling liquid temperature, A is the surface area, A_c is the cross-sectional area of the tubular reactor. The notation for other parameters follows those in CSTRs and is omitted here. The manipulated input (i.e., control) in this system are represented by $\Delta T_c = T_c - T_{c_s}$. T , C_A , ΔT_c are evenly sampled from $[300, 500]$ K, $[0.5, 3]$ kmol/m³, and $[100, 300]$ K, respectively.

In the context of PFR modeling, to maintain uniform input dimensions akin to CSTRs and BRs, we implement padding on the inputs for PFRs. Furthermore, we exclusively monitor the output from a single discretized location over the sampling period. Specifically, in this study, we focus on tracking the output from the first discretized point, where $N = 1$. Consequently, the final inputs comprise $[T_t, C_{A_t}, T_{c_t}, T_{c_t}]$ at the current time step t , while the outputs encapsulate the state trajectory $[T_{t+1, \dots, n}, C_{A_{t+1, \dots, n}}]$ over the subsequent n time steps (i.e., representing a one-to-many sequence problem). Leveraging parameter values randomly drawn from the range delineated in Table 3 in Appendix B, and employing the material and energy balance equations depicted in Eq. (7), we conduct numerical simulations of diverse PFRs to collect their respective output sequences, which involve employing the explicit Euler method with an integration time step of $h_c = 0.01$ hr, relative to a sampling period of $\Delta = 0.1$ hr.

The PFR physics-informed loss function is the weighted sum of data-driven loss term \mathcal{L}_d and physics-informed loss term \mathcal{L}_p . \mathcal{L}_d and \mathcal{L}_p take similar forms as those for CSTRs (i.e., Eq. (3)) but with different $\mathcal{L}_{C_{A_{t+i}}}$ and $\mathcal{L}_{T_{t+i}}$, where

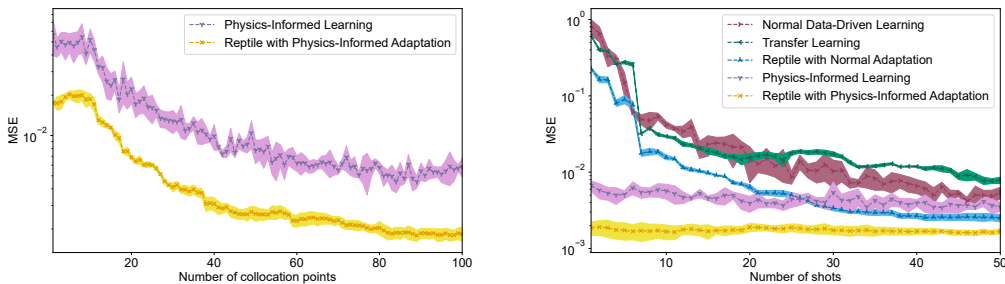
$$\mathcal{L}_{C_{A_{t+i}}} = \frac{d\widetilde{C}_{A_{t+i}}}{dt} + u \frac{\widetilde{C}_{A_{t+i}} - C_{A_t}}{Z_1 - Z_0} + k_0 e^{\frac{-E}{RT_{t+i}}} \widetilde{C}_{A_{t+i}} \quad (8a)$$

$$\mathcal{L}_{T_{t+i}} = \frac{d\widetilde{T}_{t+i}}{dt} + u \frac{\widetilde{T}_{t+i} - T_t}{Z_1 - Z_0} - \frac{-\Delta H}{\rho_L C_p} k_0 e^{\frac{-E}{RT_{t+i}}} \widetilde{C}_{A_{t+i}} - \frac{U}{\rho_L C_p A} A_c (T_{c_t} - \widetilde{T}_{t+i}) \quad (8b)$$

The calculation of the physics-informed loss term follows the method for CSTRs and BRs. Specifically, we utilize the actual values of L , N , T_{c_s} , A , A_c , u , and U , and estimate the values of k_0 , E , ΔH , C_p , and ρ_L (i.e., using the median values of k_0 , E , ΔH , C_p , and ρ_L from their respective sampling ranges shown in Table 3) in Appendix B in Eq. (8) for model adaptation.

4 Experiment results

We initiate the meta-training phase by training the Reptile-based foundation model on 500 CSTRs, 500 BRs, and 500 PFRs with different parameters representing various reactions in different settings of reactors (e.g., reactor size, flow rate, etc.). Following this, in the meta-testing phase, we evaluate the few-shot performance of the pre-trained foundation model on 5 previously unseen CSTRs, 5



(a) 10-shot performance with respect to different number of collocation points on unseen CSTRs.

(b) Few-shot performance on unseen CSTRs.

Figure 3: Performance of few-shot adaptation to unseen CSTRs.

previously unseen BRs, and 5 previously unseen PFRs, respectively, using MSE as the evaluation metric. Specifically, during meta-testing, we fine-tune the foundation model using a limited number of samples from the designated reaction and assess its performance by computing the MSE over all samples from the same reaction, where the samples used for few-shot fine-tuning and the collocation points are randomly selected from the whole operational region of the designated reaction.

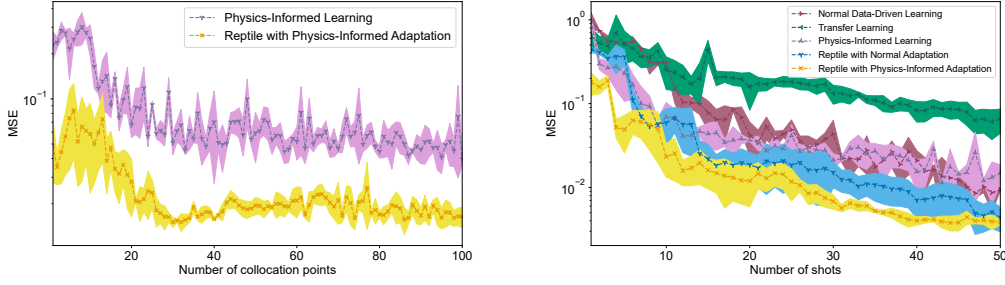
We employ a 2-layer RNN with 64 neurons per layer and ReLU activation functions as the foundation model architecture. The model is optimized using the Adam optimizer. Based on our previous experiments, we observed that a testing MSE on the order of 10^{-3} is indicative of satisfactory performance, rendering the model suitable for applications in process systems engineering. A further discussion on how to achieve lower testing MSE and the rationale for choosing simple RNNs as the base architecture instead of other high-performing recurrent units can be found in Appendix C.4.

In the following subsections, we will provide a comprehensive analysis of the few-shot performance with respect to five different approaches on unseen CSTRs, BRs, and PFRs respectively, namely Normal Data-Driven Learning, Transfer Learning, Reptile-Based Foundation Model with Normal Data-Driven Adaptation, Physics-Informed Learning, and Reptile-Based Foundation Model with Physics-Informed Adaptation. These approaches vary in their use of prior knowledge, meta-learning techniques, and incorporation of physics-based constraints. By comparing their few-shot performance, we can assess which method is most effective for the given tasks and dataset. A comprehensive description of the setup for these five approaches is provided in Appendix B and a description of computing resources is provided in Appendix C.5.

4.1 Few-shot adaptation to unseen CSTRs

First, we explore how varying the number of collocation points affects model performance in a few-shot setting. As depicted in Fig. 3a, with a fixed number of shots at 10, we observe that PI-based approaches reach convergence at around 80 collocation points. Further increasing the number of collocation points does not lead to additional learning. Instead, additional input-output pairs (i.e., increasing the number of shots) are necessary to continue improving the model.

Next, we explore how the number of shots influences model performance across the five aforementioned approaches (i.e., we use 100 collocation points for PI-based methods). From Fig. 3b, it is evident that the transfer learning approach exhibits the poorest performance. This is because the model encounters confusion during the pre-training phase using conventional learning algorithms, given the disparate distributions of CSTRs, BRs, and PFRs. Conventional physics-informed learning (i.e., without reptile model) starts with a strong foundation but halts its learning process due to the limited additional information provided by the constrained number of shots, eventually matching the performance of normal data-driven learning with around 50 shots. Reptile with normal adaptation surpasses physics-informed learning after around 30 shots and requires over 15 shots to achieve satisfactory performance (i.e., reaching an MSE magnitude of 10^{-3}). In contrast, Reptile with physics-informed adaptation reaches a comparable level with just about 1 shot. Notably, Reptile with physics-informed adaptation maintains the lowest MSE consistently as the number of shots increases.



(a) 10-shot performance with respect to different number of collocation points on unseen BRs.

(b) Few-shot performance on unseen BRs.

Figure 4: Performance of few-shot adaptation to unseen BRs.

4.2 Few-shot adaptation to unseen BRs

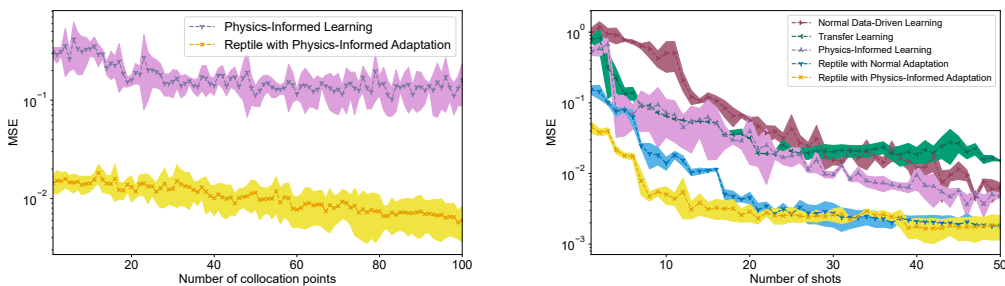
First, we investigate how adjusting the number of collocation points influences model performance within a few-shot setting. Similarly to the observations made for CSTRs, illustrated in Fig. 4a, when maintaining a fixed number of shots at 10, we find that PI-based approaches converge at approximately 80 collocation points. However, additional increments in the number of collocation points do not yield further learning benefits. Instead, for continued model enhancement, additional input-output pairs (i.e., increasing the number of shots) are required. Furthermore, in contrast to CSTRs, BRs prove to be more challenging to train using PI-based methods. As illustrated in Fig. 4a, both PI-based approaches exhibit significant fluctuations, suggesting high sensitivity to the quality of selected collocation points, which aligns with the findings in [25].

Next, we investigate how the number of shots influences model performance across the five aforementioned approaches (i.e., using 100 collocation points for PI-based methods). From Fig. 4b, it is apparent that the transfer learning approach performs the poorest, due to confusion during the pre-training phase caused by the distinct distributions of CSTRs, BRs, and PFRs. Conventional physics-informed learning begins with a robust foundation but stalls in its learning trajectory due to the limited additional information from the constrained number of shots, eventually matching normal data-driven learning performance with approximately 25 shots. More importantly, consistent with earlier findings, it is more challenging to train BRs using PI-based methods compared to CSTRs. Reptile with normal adaptation requires roughly 40 shots to achieve satisfactory performance (i.e., reaching an MSE magnitude of 10^{-3}). Conversely, Reptile with physics-informed adaptation attains a similar level with only about 25 shots. Notably, Reptile with physics-informed adaptation consistently maintains the lowest MSE as the number of shots increases.

4.3 Few-shot adaptation to unseen PFRs

First, we explore how adjusting the number of collocation points influences model performance within a few-shot setting. As depicted in Fig. 5a, when maintaining a fixed number of shots at 10, we observe that physics-informed learning converges at approximately 50 collocation points, and Reptile with physics-informed adaptation shows little improvement at around 100 collocation points. However, further increases in the number of collocation points do not lead to significant learning benefits. Instead, continued model enhancement requires additional input-output pairs (i.e., increasing the number of shots). Moreover, unlike CSTRs, PFRs present greater challenges when trained using PI-based methods. As illustrated in Fig. 5a, both PI-based approaches exhibit significant fluctuations, indicating a high sensitivity to the quality of selected collocation points.

Next, we examine how the number of shots influences model performance across the five aforementioned approaches (i.e., with 100 collocation points for PI-based methods). From Fig. 5b, it is evident that, similar to the previous two cases, the transfer learning approach performs the poorest (i.e., as indicated by its consistently high MSE, particularly when the number of shots exceeds 40). Additionally, conventional physics-informed learning stalls in its learning trajectory due to the limited additional information from the constrained number of shots, and eventually matches normal data-driven learning performance with approximately 50 shots. Furthermore, in line with earlier findings, training PFRs using PI-based methods proves more challenging compared to CSTRs. However, Rep-



(a) 10-shot performance with respect to different number of collocation points on unseen PFRs.

(b) Few-shot performance on unseen PFRs.

Figure 5: Performance of few-shot adaptation to unseen PFRs.

tile with normal adaptation requires approximately 17 shots to achieve satisfactory performance (i.e., reaching an MSE magnitude of 10^{-3}), whereas Reptile with physics-informed adaptation reaches a comparable level with only about 7 shots. Notably, Reptile with physics-informed adaptation consistently maintains the lowest MSE as the number of shots increases.

5 Limitations and future works

The analysis presented in Section 4 demonstrates that physics-informed learning provides the model with a solid starting point, while Reptile-based meta-training initializes the model effectively based on previously acquired knowledge. By combining these approaches, we have developed a foundation model capable of adapting to various unseen chemical reactions, including CSTRs, BRs, and PFRs, with few-shot adaptation. However, the efficacy of our proposed method is heavily influenced by the challenges associated with training PI-based methods for specific tasks. Notably, BRs and PFRs pose greater difficulty for PI-based training, resulting in less discernible differences between our Reptile-based foundation model with physics-informed adaptation and the one with normal data-driven adaptation, compared to CSTRs, where the distinction is more pronounced. The challenge of training BRs, PFRs, and possibly CSTRs in a physics-informed approach may stem from our use of estimated parameter values rather than precise ones to compute the physics-informed loss term.

Additionally, our current foundation model exclusively focuses on elementary reactions. Future iterations will incorporate more complex reactions, such as multi-step and multi-component reactions, to enhance its applicability. Furthermore, since we utilize a single model as the foundation, ensuring consistent input and output dimensions across all reactions is necessary, restricting its versatility. Future endeavors will explore alternative methodologies, such as modular deep learning [26], to accommodate reactions with varying input and output dimensions.

Lastly, this work is simulation-based due to the lack of public datasets, unlike computer vision and natural language processing, which benefit from publicly shared data through academic research and open-access journals. This is because chemical engineering deals with large-scale industrial processes, where data collection is complex, proprietary, and highly variable. Companies consider this data proprietary and competitive, so it is rarely shared publicly.

6 Conclusion

In this study, we introduce a novel application of foundation models in nonlinear chemical process modeling. By leveraging the meta-learning algorithm Reptile and physics-informed adaptation, we have developed a foundation model for rapid adaptation to previously unseen chemical reactions in CSTRs, BRs, and PFRs, with just a few training shots. The proposed method surpasses conventional approaches such as data-driven learning, physics-informed learning, transfer learning, and meta-learning in a few-shot setting. The successful implementation of the proposed foundation model holds the potential to revolutionize chemical reaction modeling by drastically reducing the data requirements and improving generalizability to new reactions. This advancement could have significant implications for various applications in chemical engineering, such as process optimization and synthesis design.

References

- [1] R. Bommasani, D. A. Hudson, E. Adeli, R. Altman, S. Arora, S. von Arx, M. S. Bernstein, J. Bohg, A. Bosselut, E. Brunskill, *et al.*, “On the Opportunities and Risks of Foundation Models,” *arXiv preprint arXiv:2108.07258*, 2021.
- [2] J. Achiam, S. Adler, S. Agarwal, L. Ahmad, I. Akkaya, F. L. Aleman, D. Almeida, J. Altschmidt, S. Altman, S. Anadkat, *et al.*, “Gpt-4 Technical Report,” *arXiv preprint arXiv:2303.08774*, 2023.
- [3] T. Brooks, B. Peebles, C. Homes, W. DePue, Y. Guo, L. Jing, D. Schnurr, J. Taylor, T. Luhman, E. Luhman, *et al.*, “Video Generation Models as World Simulators, 2024,” URL <https://openai.com/research/video-generation-models-as-world-simulators>.
- [4] S. Takeda, A. Kishimoto, L. Hamada, D. Nakano, and J. R. Smith, “Foundation Model for Material Science,” in *Proceedings of the AAAI Conference on Artificial Intelligence*, vol. 37, pp. 15376–15383, 2023.
- [5] W. Ahmad, E. Simon, S. Chithrananda, G. Grand, and B. Ramsundar, “Chemberta-2: Towards Chemical Foundation Models,” *arXiv preprint arXiv:2209.01712*, 2022.
- [6] Y. Yang, R. Shi, Z. Li, S. Jiang, Y. Yang, B.-L. Lu, and H. Zhao, “BatGPT-Chem: A Foundation Large Model for Chemical Engineering,” 2024.
- [7] F. Lanusse, L. Parker, S. Golkar, M. Cranmer, A. Bietti, M. Eickenberg, G. Krawezik, M. McCabe, R. Ohana, M. Pettee, *et al.*, “AstroCLIP: Cross-Modal Pre-Training for Astronomical Foundation Models,” *arXiv preprint arXiv:2310.03024*, 2023.
- [8] M. McCabe, B. R.-S. Blancard, L. H. Parker, R. Ohana, M. Cranmer, A. Bietti, M. Eickenberg, S. Golkar, G. Krawezik, F. Lanusse, *et al.*, “Multiple Physics Pretraining for Physical Surrogate Models,” *arXiv preprint arXiv:2310.02994*, 2023.
- [9] B. Decardi-Nelson, A. S. Alshehri, A. Ajagekar, and F. You, “Generative AI and Process Systems Engineering: The Next Frontier,” *Computers & Chemical Engineering*, p. 108723, 2024.
- [10] S. Horawalavithana, E. Ayton, S. Sharma, S. Howland, M. Subramanian, S. Vasquez, R. Cosbey, M. Glenski, and S. Volkova, “Foundation Models of Scientific Knowledge for Chemistry: Opportunities, Challenges and Lessons Learned,” in *Proceedings of BigScience Episode# 5–Workshop on Challenges & Perspectives in Creating Large Language Models*, pp. 160–172, 2022.
- [11] M. Livne, Z. Miftahutdinov, E. Tutubalina, M. Kuznetsov, D. Polykovskiy, A. Brundyn, A. Jhunjhunwala, A. Costa, A. Aliper, and A. Zhavoronkov, “nach0: Multimodal Natural and Chemical Languages Foundation Model,” *arXiv preprint arXiv:2311.12410*, 2023.
- [12] Z. Wu, A. Tran, D. Rincon, and P. D. Christofides, “Machine Learning-Based Predictive Control of Nonlinear Processes. Part I: Theory,” *AIChE Journal*, vol. 65, no. 11, p. e16729, 2019.
- [13] Z. Wu, A. Tran, D. Rincon, and P. D. Christofides, “Machine-Learning-Based Predictive Control of Nonlinear Processes. Part II: Computational Implementation,” *AIChE Journal*, vol. 65, no. 11, p. e16734, 2019.
- [14] Z. Wang and Z. Wu, “Input Convex LSTM: A Convex Approach for Fast Lyapunov-Based Model Predictive Control,” *arXiv preprint arXiv:2311.07202*, 2023.
- [15] M. Xiao, C. Hu, and Z. Wu, “Modeling and Predictive Control of Nonlinear Processes using Transfer Learning Method,” *AIChE Journal*, vol. 69, no. 7, p. e18076, 2023.
- [16] M. Xiao, K. Vellayappan, P. Pravin, K. Gudena, and Z. Wu, “Optimization-Based Multi-Source Transfer Learning for Modeling of Nonlinear Processes,” *Chemical Engineering Science*, p. 120117, 2024.
- [17] F. Zhuang, Z. Qi, K. Duan, D. Xi, Y. Zhu, H. Zhu, H. Xiong, and Q. He, “A Comprehensive Survey on Transfer Learning,” *Proceedings of the IEEE*, vol. 109, no. 1, pp. 43–76, 2020.

- [18] A. Nichol and J. Schulman, “Reptile: A Scalable Metalearning Algorithm,” *arXiv preprint arXiv:1803.02999*, vol. 2, no. 3, p. 4, 2018.
- [19] C. Finn, P. Abbeel, and S. Levine, “Model-Agnostic Meta-Learning for Fast Adaptation of Deep Networks,” in *International conference on machine learning*, pp. 1126–1135, PMLR, 2017.
- [20] C. Finn, K. Xu, and S. Levine, “Probabilistic Model-Agnostic Meta-Learning,” *Advances in neural information processing systems*, vol. 31, 2018.
- [21] C. Finn, A. Rajeswaran, S. Kakade, and S. Levine, “Online Meta-Learning,” in *International conference on machine learning*, pp. 1920–1930, PMLR, 2019.
- [22] M. Khodak, M.-F. F. Balcan, and A. S. Talwalkar, “Adaptive Gradient-Based Meta-Learning Methods,” *Advances in Neural Information Processing Systems*, vol. 32, 2019.
- [23] A. Rajeswaran, C. Finn, S. M. Kakade, and S. Levine, “Meta-Learning with Implicit Gradients,” *Advances in neural information processing systems*, vol. 32, 2019.
- [24] A. Nichol, J. Achiam, and J. Schulman, “On First-Order Meta-Learning Algorithms,” *arXiv preprint arXiv:1803.02999*, 2018.
- [25] P. Rathore, W. Lei, Z. Frangella, L. Lu, and M. Udell, “Challenges in Training PINNs: A Loss Landscape Perspective,” *arXiv preprint arXiv:2402.01868*, 2024.
- [26] J. Pfeiffer, S. Ruder, I. Vulić, and E. M. Ponti, “Modular Deep Learning,” *arXiv preprint arXiv:2302.11529*, 2023.
- [27] S. Hochreiter and J. Schmidhuber, “Long Short-Term Memory,” *Neural computation*, vol. 9, no. 8, pp. 1735–1780, 1997.
- [28] T. K. Rusch and S. Mishra, “Unicornn: A Recurrent Model for Learning very Long Time Dependencies,” in *International Conference on Machine Learning*, pp. 9168–9178, PMLR, 2021.
- [29] A. Orvieto, S. L. Smith, A. Gu, A. Fernando, C. Gulcehre, R. Pascanu, and S. De, “Resurrecting Recurrent Neural Networks for Long Sequences,” in *International Conference on Machine Learning*, pp. 26670–26698, PMLR, 2023.
- [30] A. Vaswani, N. Shazeer, N. Parmar, J. Uszkoreit, L. Jones, A. N. Gomez, Ł. Kaiser, and I. Polosukhin, “Attention is All You Need,” *Advances in neural information processing systems*, vol. 30, 2017.

A Reptile

The primary aim of meta-training is to expose the model to a wide range of tasks, enabling it to learn initial parameters conducive to rapid adaptation to new, unseen tasks. In this phase, Reptile optimizes the model’s parameters to facilitate efficient adaptation to different tasks with minimal updates. Essentially, Reptile guides the model towards a solution θ that closely approximates the optimal solutions manifold for each task τ in Euclidean distance, converging through repeated sampling of task batches, model updates, and parameter adjustments.

At its core, Reptile emphasizes the acquisition of swift task learning capabilities rather than specialization in a single task. It embodies meta-learning, where the model learns how to learn. Throughout meta-training, the model encounters diverse tasks and refines a parameter set optimized for quick adaptation to new challenges. By concurrently exposing the model to various tasks, Reptile identifies shared features among them, contrasting with conventional neural networks focused on fitting individual tasks. The result of this meta-learning process is the derivation of adaptable parameters represented by θ . Remarkably, these parameters demonstrate remarkable flexibility, requiring minimal gradient steps for fine-tuning to new tasks. Reptile’s strength lies in its ability to generalize across tasks and swiftly adapt to novel challenges, making it a robust meta-learning framework. Analogously, Reptile operates akin to a **tug-of-war** scenario, where task groups exert force in different directions, striving to establish equilibrium, ultimately achieving a balanced state in the system (i.e., a concept reminiscent of static equilibrium in Physics).

Algorithm 2 Reptile-based Foundation Model Meta-Training

Require: $p(\mathcal{T})$: distribution over tasks;
Require: ϵ : meta-optimization step size hyperparameter;
Require: α : linear schedule step size hyperparameter;
Require: x, y : training inputs and outputs respectively;
Require: *Model* : a neural network;

- 1: Initialize θ ; $\triangleright \theta$ is the initial parameters of the model
- 2: **for** $iteration \leftarrow 1, 2, \dots, n_{tasks}$ **do**
- 3: Sample one task $\tau \sim p(\mathcal{T})$;
- 4: **for** $innerepoch \leftarrow 1, 2, \dots, n_{epochs}$ **do**
- 5: Let $\tilde{\theta} \leftarrow \theta$;
- 6: **for** $i \leftarrow 1, 2, \dots, n_{batches}$ **do**
- 7: $\tilde{y}_i \leftarrow Model(x_i)$; $\triangleright \tilde{y}_i$ is the predicted output w.r.t current batch of input x_i
- 8: Compute loss $\mathcal{L}_{\tau_i}(\tilde{y}_i, y_i)$ w.r.t. current batch;
- 9: Update $\tilde{\theta} \leftarrow Adam(\mathcal{L}_{\tau_i}(\tilde{y}_i, y_i), \tilde{\theta})$;
- 10: **end for**
- 11: Compute $\alpha \leftarrow \epsilon(1 - \frac{iteration}{n_{tasks}})$;
- 12: Update $\theta \leftarrow \theta + \alpha(\tilde{\theta} - \theta)$;
- 13: **end for**
- 14: **end for**

Table 1: Parameter value ranges of CSTRs.

$F = [0, 55] \text{ m}^3/\text{hr}$	$E = [4.75, 5.25] \times 10^4 \text{ kJ/kmol}$	$T_0 = [0, 600] \text{ K}$
$R = 8.314 \text{ kJ/kmol K}$	$C_{A0s} = [0, 8] \text{ kmol/m}^3$	$Q_s = 0.0 \text{ kJ/hr}$
$\rho_L = [950, 1050] \text{ kg/m}^3$	$C_p = [0.219, 0.243] \text{ kJ/kg K}$	$V = [0, 11] \text{ m}^3$
$k_0 = [8.04, 8.88] \times 10^6 \text{ m}^3/\text{kmol hr}$	$\Delta H = [-1.21, -1.09] \times 10^4 \text{ kJ/kmol}$	

Table 2: Parameter value ranges of BRs.

$V = [0, 11] \text{ m}^3$	$R = 8.314 \text{ kJ/kmol K}$
$C_p = [0.219, 0.243] \text{ kJ/kg K}$	$E = [4.75, 5.25] \times 10^4 \text{ kJ/kmol}$
$E = [4.75, 5.25] \times 10^4 \text{ kJ/kmol}$	$\rho_L = [950, 1050] \text{ kg/m}^3$
$k_0 = [0, 9.31] \times 10^8 \text{ m}^3/\text{kmol hr}$	$\Delta H = [-1.21, -1.09] \times 10^4 \text{ kJ/kmol}$

B Experiment setup

The PFR dynamic model is described by the following material and energy balance equations:

$$\frac{\partial C_A}{\partial t} = -u \frac{\partial C_A}{\partial z} - k_0 e^{-\frac{E}{RT}} C_A, \quad \frac{\partial T}{\partial t} = -u \frac{\partial T}{\partial z} + \frac{-\Delta H}{\rho_L C_p} k_0 e^{-\frac{E}{RT}} C_A + \frac{U}{\rho_L C_p A} A_c (T_c - T)$$

The parameter value ranges of CSTRs, BRs, and PFRs are described in Table 1, Table 2, and Table 3 respectively.

We assess the performance of five different approaches in a few-shot setting, formulated as follows:

- **Normal Data-Driven Learning:** This approach involves training a randomly initialized model directly with few-shot samples. It is a standard method where the model learns solely from the provided data without any prior knowledge or pre-training.
- **Transfer Learning:** Here, the model is pre-trained on a large dataset containing 500 CSTRs, 500 BRs, and 500 PFRs. This pre-training phase helps the model learn general features and patterns from the data. Then, the pre-trained model is fine-tuned with few-shot samples, allowing it to adapt to specific tasks more efficiently. However, the key difference between transfer learning and meta-learning is that transfer learning focuses on transferring knowledge from one specific task to another related task and develops the pre-trained model following conventional learning algorithms, while meta-learning aims to develop novel learning algorithms such as Reptile that can learn the common pattern across a variety of tasks or domains such that the models can quickly adapt to a new process.
- **Reptile-Based Foundation Model with Normal Data-Driven Adaptation:** In this method, the model is first pre-trained on the 500 CSTRs, 500 BRs, and 500 PFRs dataset using the Reptile learning rule. After pre-training, the foundation model is fine-tuned with few-shot samples in a normal data-driven manner.
- **Physics-Informed Learning:** Similar to normal data-driven learning, this approach involves training a randomly initialized model directly with few-shot samples. However, during the training process, a physics-informed loss function is utilized. This loss function incorporates domain-specific knowledge or physical constraints into the learning process, potentially leading to improved generalization and robustness.
- **Reptile-Based Foundation Model with Physics-Informed Adaptation:** This method combines the benefits of both Reptile-based meta-learning and physics-informed learning. The model is initially pre-trained on the 500 CSTRs, 500 BRs, and 500 PFRs dataset using the Reptile learning rule to enhance its adaptability. Then, during fine-tuning with few-shot samples, a physics-informed loss function is employed to leverage domain-specific knowledge.

Table 3: Parameter value ranges of PFRs.

$A = [0, 0.022] m^2$	$A_c = [0, 0.11] m^2$	$L = 1 m$
$u = [0, 4] m/min$	$U = [0, 50] kcal/m^2 K$	$N = 10$
$\rho_L = [950, 1050] kg/m^3$	$R = 8.314 kJ/kmol K$	$T_{cs} = [273, 586] K$
$C_p = [0.219, 0.243] kJ/kg K$	$E = [4.75, 5.25] \times 10^4 kJ/kmol$	
$k_0 = [8.04, 8.88] \times 10^6 m^3/kmol hr$	$\Delta H = [-1.21, -1.09] \times 10^4 kJ/kmol$	

C Further discussions

C.1 Discussion on PINNs

In the context of physics-informed neural networks (PINNs), a collocation point refers to a specific location within the domain of interest where the governing physics equations are enforced as part of the training process. PINNs combine traditional numerical methods for solving ordinary differential equations (ODEs) or partial differential equations (PDEs) with neural networks, allowing for the solution of complex physical problems directly from data. Collocation points are strategically chosen locations within the domain where the ODEs or PDEs are expected to hold true. By enforcing the ODEs or PDEs at these points during training, PINNs learn to approximate the solution of the underlying physical system while also fitting available data. Collocation points are typically selected based on the underlying physics of the problem and the geometry of the domain. Their distribution and density can influence the accuracy and stability of the PINN solution. A comprehensive analysis on the challenges in training PINNs can be found in [25].

C.2 Discussion on reactor modeling

It is essential to highlight that we enforce constraints on the simulated output trajectories for all CSTRs, BRs, and PFRs, to ensure them within a plausible range. This measure is crucial for ensuring that the simulated CSTRs, BRs, and PFRs adhere to theoretical validity.

Furthermore, the integration time step and sampling period vary across CSTRs, BRs, and PFRs in this simulation study. However, it is important to note that the foundation model can accommodate differing integration time steps and sampling periods for real-world reactors, provided the input dimensions remain consistent. This is due to the fact that the inputs to the neural network are merely numerical values, lacking any inherent physical interpretation for the network.

C.3 Discussion on physics-informed loss function

The terms $\frac{d\widetilde{C}_{At+i}}{dt}$ and $\frac{d\widetilde{T}_{t+i}}{dt}$ in \mathcal{L}_p of CSTRs, BRs, and PFRs, can be computed using numerical methods such as Euler method. For example,

$$\frac{d\widetilde{C}_{At+i}}{dt} = \frac{\widetilde{C}_{At+i+k} - \widetilde{C}_{At+i}}{kh_c}, \quad \frac{d\widetilde{T}_{t+i}}{dt} = \frac{\widetilde{T}_{t+i+k} - \widetilde{T}_{t+i}}{kh_c}$$

Moreover, training PINNs can be notably challenging, and their performance is highly sensitive to the hyperparameter γ governing the weighting of the loss function. In summary, the physics-informed loss term of CSTR, BR, and PFR can be expressed as follows:

$$\mathcal{L}_p = \gamma_1 \mathcal{L}_d + \gamma_2 \mathcal{L}_{C_A} + \gamma_3 \mathcal{L}_T$$

where $\gamma_1 = 1 \times 10^3$, $\gamma_2 = 1 \times 10^{-2}$, and $\gamma_3 = 1 \times 10^{-5}$ give the best performance for all three types of reactors.

C.4 Discussion on model performance

For applications requiring extremely low MSE on the order of 10^{-4} or 10^{-5} , utilizing high-performing RNNs such as Long Short-Term Memory (LSTM) [27], UniCORNN [28], and Linear Recurrent Units [29], or even Transformers [30], is advisable over traditional RNNs. However, these advanced models come with a trade-off in computational efficiency. From an engineering standpoint, simplicity

is crucial for ensuring that the model can be easily integrated into existing industrial systems. Since simple RNNs can deliver satisfactory performance, this work aims to develop a network architecture based on simple RNNs that balances simplicity with adequate accuracy, rather than solely pursuing the optimal model architecture for accuracy.

Additionally, increasing the number of collocation points can improve model performance but significantly increases computational complexity, as indicated by the rise in the number of floating-point operations. In this work, we aim to maintain system simplicity to ensure computational efficiency, seeking a balance between computational efficiency and achieving a reasonable MSE for future real-time applications, such as neural network-based MPC.

C.5 Computational resources

The experiments were conducted on the NVIDIA Quadro RTX A5000 GPU of 24 GB memory, but they are also compatible with CPUs equipped with at least 64 GB of RAM. A single run for meta-training took about 48 hours using CPU with 64 GB of RAM.